

Reactions of alkaline earth metals and nitrogen in sealed niobium ampoules: the formation of $MgZn_2$ type intermetallic phases in the presence of nitrogen and the new compound $Ba_5[NbN_4]N$

Olaf Reckeweg^{a,b,*}, Cora Lind^c, Arndt Simon^a, Francis J. DiSalvo^b

^a Max-Planck-Institut für Festkörperforschung, Heisenbergstr. 1, D-70569 Stuttgart, Germany

^b Baker Laboratory, Department of Chemistry and Chemical Biology, Cornell University, Ithaca, NY 14853-1301, USA

^c Department of Chemistry, MS 602, University of Toledo, Toledo, OH 43606-3390, USA

Received 8 December 2003; received in revised form 12 April 2004; accepted 12 April 2004

Abstract

Reactions between alkaline earth metals or their corresponding nitrides and NaN_3 as nitrogen donor in cleaned sealed Nb ampoules at different temperatures yields known phases, ' β - Ca_3N_2 ' and single crystals in the form of transparent, orange plates of $Ba_5[NbN_4]N$. The crystal structure of this new compound was determined by means of single crystal X-ray diffraction ($C2/m$ (no. 12), $a = 1231.7(3)$, $b = 1094.6(2)$, $c = 853.8(2)$ pm, $\beta = 113.65(3)^\circ$ and $Z = 4$). At temperatures $\geq 1000^\circ C$, the available nitrogen apparently reacts with the Nb container walls and intermetallic phases are formed. The crystal structures of $AeMg_2$ ($MgZn_2$ type with $Ae = Ca, Yb, Sr, Eu$ and Ba) were re-determined by X-ray single crystal structure analyses on crystals obtained in such reactions to ascertain the presence or absence of nitrogen in structural voids. The structures of the ternary nitride and intermetallic phases are described and compared to known compounds. © 2004 Elsevier B.V. All rights reserved.

Keywords: Alkaline earth metal; Niobium; Nitride; $MgZn_2$; Laves phase; Structure elucidation

1. Introduction

Many different reaction techniques have been employed for the syntheses of nitrides. They can roughly be divided into sealed- and open-vessel, the latter with flow-by or flow-through of a nitrogen source. Both strategies have their specific advantages and disadvantages, which will not be discussed here. Regardless of the strategy employed, cleaned niobium and tantalum are frequently used as 'inert' container materials. However, in many cases the container material is incorporated into the reaction products, e.g. in the case of $Ba(Mg_{3.33}M_{0.67})N_4$ ($M = Nb$ or Ta) [1].

In an attempt to better understand the reactivity of the container materials, we carried out a series of reactions where alkaline earth metals and/or alkaline earth metal nitride reactants were sealed in niobium ampoules with NaN_3 as a

source of readily available nitrogen. The products obtained were determined as a function of the reaction temperature. Ytterbium and europium, which frequently show behavior very similar to alkaline earth metals in nitride compounds, were included in the list of alkaline earth metals for convenience. The results of this series of reactions are presented here.

Structural refinements on X-ray single crystal data of $AeMg_2$ ($Ae = Ca, Yb, Sr, Eu$ and Ba) alloys (which were among the products of some reactions) were used to address the potential presence of nitrogen in structural voids. No nitrogen is detected in these intermetallic phases.

2. Experimental section

All manipulations were carried out under a continuously purified and monitored argon atmosphere in glove boxes. The reactions took place in thoroughly cleaned (cleaning bath consists of 4:2:1 volume ratio of H_2SO_4 (conc.), HNO_3 (fuming) and HF (40%)) arc-welded Nb tubes (99.99%, Plansee, Germany).

* Corresponding author. Tel.: +1-607-255-4164;
fax: +1-607-255-4137.
E-mail address: fjd3@cornell.edu (O. Reckeweg).

Mg (chips, 99.98%, Aldrich), Ca (<20 ppmw C, <30 ppmw H and <100 ppmw O, dendritic pieces, Ames Laboratory, Materials Preparation Center), Sr (99.95%, dendritic pieces, Strem), Ba (99.9%, dendritic, Strem), Eu (99.9%, powder), and Yb (99.9%, sublimed dendritic) were used as received, NaN_3 (99%, powder, Aldrich) was dried at 400 K under dynamic vacuum for 2 h prior to use, Mg_3N_2 , Ca_3N_2 , Sr_2N , Ba_2N , EuN and YbN were synthesized following literature methods [2,3]. To verify the nature of these binary nitrides, powder X-ray diffractograms of all products were recorded on an Inel powder diffractometer (ground materials were loaded in 0.2 mm, thin-walled glass capillaries). No impurities were detected by this method unless stated otherwise.

The reactions were carried out in the following manner: stoichiometric amounts of the starting materials ($\sum m \approx 500$ mg, the nitrogen content as indicated by the nominal starting composition was supplied by the addition of proper amounts of NaN_3 if necessary) as listed in Table 1 were filled in cleaned niobium ampoules of about 5 cm length without compacting or grinding the starting materials. The arc-welded metal tubes were enclosed in evacuated and fused silica tubes to protect the metal containers from oxidation by air during heating. The reaction vessels were placed upright in a box furnace, which was heated within 24 h to reaction temperatures of 600, 800, 1000 or 1200 °C. The samples were kept at the respective temperature for 3 days. Then the furnace was switched off and allowed to cool to room temperature. The higher the reaction temperature was set, the more brittle the metal container became and the more the Nb lost its metallic luster on the inner and outer tube surfaces.

2.1. Ba_5NbN_5

Ba_2N and NaN_3 (mixed in a 1:2 molar ratio ($\sum m \approx 420$ mg) and sealed inside an arc-welded niobium container which was enclosed inside an evacuated silica tube) were heated to 625 °C within 24 h. After 10 days at this temperature, the furnace was cooled to room temperature over a period of 24 h. The reaction product contained mainly unreacted Ba_2N as identified by its X-ray powder pattern, metallic Na and some dark orange, transparent plates of only moderate crystallinity.

3. X-ray investigations

To verify the nature of the products, powder X-ray diffractograms of all products were measured on an Inel powder diffractometer (ground materials were loaded and sealed in 0.2 mm, thin-walled glass capillaries). Suitable single crystals of $\text{Ba}_5[\text{NbN}_4]\text{N}$ and of the Laves phases of the MgZn_2 type (AeMg_2 with $\text{Ae} = \text{Ca}, \text{Yb}, \text{Sr}, \text{Eu}$ and Ba) were selected in an argon filled glove box under a microscope and sealed in thin-walled glass capillaries. The crystals were checked for their quality by taking rotation frames on a

Bruker Smart CCD using $\text{Mo K}\alpha$ radiation. If the quality was found to be sufficient, a set of intensity data was collected on the same machine. All processing of the data, the structure solutions and refinements were carried out using Bruker Smart CCD software [4]. Selected parameters of the measurements and results of the refinements are summarized in Tables 1–4. Further details of the crystal structure investigations may be obtained from the Fachinformationszentrum Karlsruhe, Eggenstein-Leopoldshafen, Germany (fax: +49-7247-808-666; e-mail: crysdata@fiz-karlsruhe.de), on quoting the depository numbers CSD-412667 ($\text{Ba}_5[\text{NbN}_4]\text{N}$), 412683 (CaMg_2), 416684 (SrMg_2), 412681 (BaMg_2), 412666 (YbMg_2) and 412689 (EuMg_2).

The compounds AeMg_2 ($\text{Ae} = \text{Ca}, \text{Yb}, \text{Sr}, \text{Eu}$ and Ba) are moderately air-stable, $\text{Ba}_5[\text{NbN}_4]\text{N}$ is air and moisture sensitive and decomposes if exposed to air.

4. Discussion

4.1. The starting materials

The identification of the binary nitrides from their respective powder diffractogram was straightforward for Mg_3N_2 [2], $\alpha\text{-Ca}_3\text{N}_2$ [2], EuN and YbN [9]. Difficulties were encountered for Ae_2N compounds ($\text{Ae} = \text{Ca}, \text{Sr}$ or Ba ; Table 5) [3,10–16]. The measured intensities differed considerably from the simulated pattern due to preferred orientation of the crystallites, which usually form as hexagonal plates. Additionally, the c lattice constants showed a strong dependence on the reaction temperature. The c axis length decreases with increasing temperature until decomposition takes place. The insertion of small amounts of hydride in the Ae_2N compounds was considered as an explanation for this phenomena [3], because a considerable decrease of the c axes can be observed due to the formation of Ae_2NH , which becomes smaller with increasing reaction temperature. However, if only small amounts of hydride are present both phases form in equilibrium with each other and are identified by their respective X-ray powder diffractogram. So the most probable explanation seems to be the insertion of nitrogen in form of diazenide (N_2^{2-}) species at lower temperature, which break up with increasing temperature [17–19]. The dependence of the length of the c axes on the reaction temperature was already reported for Ca_2N [3,10–12], and inspection of the literature reveals variations of the c lattice parameters for Sr_2N [3,13,14] and Ba_2N [3,8,15,16] as well. Table 5 shows the range of the lattice constants that have been reported so far.

4.2. The behavior of alkaline earth metals with nitrogen in sealed niobium containers

The results of our experiments on the reaction of alkaline earth metals with nitrogen in sealed Nb containers are shown in Table 6. Table 7 gives an overview of selected physical

Table 1
Parameters of the X-ray single crystal structure determinations and selected bond length of MgZn₂ type compounds

	Compounds				
	CaMg ₂	YbMg ₂	SrMg ₂	EuMg ₂	BaMg ₂
CSD-number	412683	412666	412684	412689	412681
Space group, Z	<i>P</i> 6 ₃ / <i>mmc</i> (#194), 4				
Lattice constant					
<i>a</i> (pm)	625.28(6)	623.38(3)	648.45(8)	638.77(9)	667.86(4)
<i>c</i> (pm)	1014.35(9)	1010.01(6)	1045.58(14)	1032.23(18)	1061.33(7)
<i>a</i> (pm)	623	624	643.9	640	664.9
<i>c</i> (pm), Refs. [5–7]	1012	1008	1049.4	1035	1067.6
<i>V</i> (Å ³)	343.45	339.91	380.75	364.75	409.97
<i>F</i> (000)	176.0	376.0	248.0	348.0	320.0
μ (mm ⁻¹)	1.89	27.57	14.21	17.25	9.74
ρ (g cm ⁻³)	1.715	4.331	2.377	3.653	3.013
Refined parameters	10	10	10	11	11
Measured/unique reflections	2417/257	6103/268	3555/473	5666/278	27455/347
Absence/restr./inconsistent refl.	0/0/0	38/0/52	0/0/0	0/0/10	35/0/186
Ranges					
<i>h, k, l</i>	–9 to 7, –9 to 8, –15 to 15	–9 to 9, –9 to 9, –14 to 14	–9 to 9, –10 to 11, –16 to 16	–9 to 9, –8 to 9, –14 to 14	–10 to 10, –10 to 10, –16 to 16
$2\theta_{\max}$	<63.96	<64.97	<81.87	<65.12	<67.17
<i>R</i> _{int}	0.0270	0.0673	0.0548	0.0340	0.0879
GooF	1.362	1.405	1.051	1.303	1.189
R1/wR2 (all data) ^a	0.0347/0.0527	0.0349/0.0694	0.0571/0.0516	0.0339/0.0568	0.0300/0.0734
Weight factors <i>x, y</i> ^b	0.0154/0.1917	0.0057/8.2440	0.0225/0	0.0000/5.8705	0.0361/1.3479
Residual electron density	0.27 (1.92 Å from Mg2), –0.23 (1.88 Å from Mg2)	2.42 (0.79 Å from Yb), –2.19 (0.48 Å from Mg1)	0.47 (1.87 Å from Mg2), –0.71 (1.20 Å from Mg1)	1.25 (1.50 Å from Eu), –1.73 (1.97 Å from Mg2)	1.48 (0.98 Å from Ba), –1.31 (0.65 Å from Ba)
4e					
6h (3x)	3.6313(8)	3.608(3)	3.7474(8)	3.691(2)	3.814(1)
6h (6x)	3.6626(4)	3.6522(2)	3.7986(4)	3.7471(5)	3.9169(3)
2a (3x)	3.6643(4)	3.6522(2)	3.7973(5)	3.7399(5)	3.9033(2)
4e (3x)	382.24(5)	380.72(4)	395.33(5)	389.14(6)	404.24(3)
4e (1x)	381.55(13)	380.87(13)	395.83(9)	391.93(13)	409.30(6)
2a					
6h (6x)	3.1262(6)	3.120(3)	3.2175(7)	3.176(3)	3.250(1)
4e (6x)	3.6643(4)	3.6522(2)	3.7973(5)	3.7399(5)	3.9033(2)
6h					
6h (2x)	3.086(2)	3.061(9)	3.235(2)	3.207(7)	3.250(4)
2a (2x)	3.1262(6)	3.120(3)	3.2175(7)	3.176(3)	3.250(1)
6h (2x)	3.166(2)	3.173(9)	3.245(2)	318.1(7)	3.429(4)
4e (2x)	3.6313(8)	3.608(3)	3.7474(8)	3.691(2)	3.814(1)
4e (4x)	3.6626(4)	3.6527(4)	3.7986(4)	3.7471(5)	3.9169(3)

^a $R1 = \sum ||F_0| - |F_c|| / \sum |F_0|$; $wR2 = [\sum w(F_0^2 - F_c^2)^2 / \sum (wF_0^2)^2]^{1/2}$.

^b The weight factor is defined as: $w = 1/[\sigma^2(F_0^2) + (xP)^2 + yP]$ with $P = [(F_0^2) + 2F_c^2]/3$.

Table 2

Crystallographic coordinates, refined site occupancy coefficients and atomic displacement parameters of the MgZn₂ type compounds

	Wyckoff site	Atom	Refined occupancy (%)	<i>x/a</i>	<i>y/b</i>	<i>z/c</i>	<i>U</i> ₁₁	<i>U</i> ₂₂	<i>U</i> ₃₃	<i>U</i> ₁₂	<i>U</i> _{eq}
CaMg ₂ [5]	4e	Ca	100(5)	1/3	2/3	0.06193(6)	160(2)	<i>U</i> ₁₁	172(3)	80(1)	164(2)
						0.063					
	2a	Mg1	100(6)	0	0	0	187(5)	<i>U</i> ₁₁	120(6)	94(2)	165(3)
	6h	Mg2	101(6)	0.83119(9)	2 <i>x</i>	0.25	174(3)	126(4)	183(4)	63(2)	166(2)
				0.833	2<i>x</i>						
	2b	“N”	0.02(40)	0	0	0.25					
YbMg ₂ [6]	4e	Yb	100(8)	1/3	2/3	0.06146(6)	162(3)	<i>U</i> ₁₁	91(4)	81(1)	139(3)
						0.063					
	2a	Mg1	100(8)	0	0	0	Refined only isotropically			122(13)	
	6h	Mg2	101(8)	0.8303(5)	2 <i>x</i>	0.25	177(14)	123(18)	122(17)	61(9)	146(8)
				0.833	2<i>x</i>						
	2b	“N”	6(7)	0	0	0.25					
SrMg ₂ [7]	4e	Sr	100(4)	1/3	2/3	0.06072(3)	160(1)	<i>U</i> ₁₁	180(1)	80(1)	166(1)
						0.07					
	2a	Mg1	102(4)	0	0	0	186(5)	<i>U</i> ₁₁	142(9)	93(3)	172(3)
	6h	Mg2	101(4)	0.8330(1)	2 <i>x</i>	0.25	185(3)	165(3)	190(5)	83(2)	182(2)
				0.83	2<i>x</i>						
	2b	“N”	7(5)	0	0	0.25					
EuMg ₂ [6]	4e	Eu	100(6)	1/3	2/3	0.06016(6)	164(2)	<i>U</i> ₁₁	167(3)	82(1)	165(2)
						0.063					
	2a	Mg1	99(7)	0	0	0	188(16)	<i>U</i> ₁₁	80(21)	94(8)	152(10)
	6h	Mg2	101(6)	0.8326(4)	2 <i>x</i>	0.25	192(11)	153(14)	169(13)	76(7)	176(6)
				0.833	2<i>x</i>						
	2b	“N”	0.3(13)	0	0	0.25					
BaMg ₂ [7]	4e	Ba	100(5)	1/3	2/3	0.05716(4)	234(2)	<i>U</i> ₁₁	246(3)	117(1)	238(2)
						0.063					
	2a	Mg1	101(5)	0	0	0	229(8)	<i>U</i> ₁₁	216(13)	115(4)	225(6)
	6h	Mg2	101(5)	0.8378(2)	2 <i>x</i>	0.25	264(7)	239(9)	233(8)	120(5)	248(4)
				0.833	2<i>x</i>						
	2b	“N”	−2.2(7)	0	0	0.25					

Coordinates in bold are literature data.

properties of Ae, AeMg₂ and Ae–Mg–N compounds for comparison. The compounds found in the X-ray powder diffractogram are listed along with the fraction of each, as estimated from the relative diffraction intensities.

If only one metal was employed with NaN₃ and the nominal starting composition was ‘AeN’, almost every reaction turned out as expected. Sr and Ba reacted readily even at low temperatures to form the subnitrides with concomitant attack of the container walls. The reaction at *T* = 600 °C yielded the first crystal of Ba₅[NbN₄]N but with very poor quality; however, we never found any evidence for this compound in the powder X-ray diffractograms showing that this is a minority phase (≤5%). At *T* = 1200 °C orange-red powders of Ae₂NbN₃ (Ae = Sr or Ba) [24,27] were found in the Sr and Ba reactions. Mg, Yb and Eu were less reactive, but formed the quite stable binary phases Mg₃N₂, YbN or EuN, respectively, above 800 °C. Ca showed higher reactivity than the previous three elements, at temperatures below approximately *T* = 650 °C black ‘β-Ca₃N₂’ formed, above this temperature the dark brown-red α-Ca₃N₂ was recovered. With increasing temperature and nitrogen loss to the container walls, increasing amounts of the subnitride Ca₂N could be found along with α-Ca₃N₂.

For the second series of reactions with the nominal composition ‘AeMg₂N₂’ the respective metals and NaN₃ as a nitrogen source were used as starting materials. The general tendency found in the first series of reactions (reactivity Sr, Ba ≫ Ca > Mg, Yb, Eu) could be observed here as well. The quite stable ternary nitrides AeMg₂N₂ (Ae = Ca, Sr) [2,25] were the first products that formed as transparent, pale yellow hexagonal plates. At higher temperature it appears that nitrogen reacts with the Nb container walls and AeMg₂ phases were obtained. The ternary nitrides AeMg₂N₂ (Ae = Ca, Sr) were stable to nitrogen loss to somewhat higher temperatures than Ae₃N₂. A few crystals of Ba(Mg_{3.33}Nb_{0.67})N₄ [1] were found in one reaction with Ba, Mg and NaN₃ at *T* = 1000 °C, but as mentioned in the literature, the crystallinity was poor and the compound could not be detected in the respective powder X-ray diffractogram.

A third series of reactions was carried out using binary nitrides as starting materials. The reactivity of the binary nitrides with Mg₃N₂ was poor with the exception of Sr₂N, which formed SrMg₂N₂ at *T* = 800 °C. Mixtures of Mg₃N₂ with YbN and EuN remained inert up to 1000 °C, at which temperature formation of AeMg₂ alloys started.

Table 3
Parameters of the X-ray single crystal structure determination on Ba₅[NbN₄]N

Compound	Ba ₅ [NbN ₄]N
Refined stoichiometry	Ba ₅ [NbN ₄]N _{0.7(1)}
Space group (no.), Z	C2/m (12), 4
CSD-number	412072
Lattice constants	
<i>a</i> , <i>b</i> , <i>c</i> (pm)	1231.7(3), 1094.6(2), 853.8(2)
<i>α</i> , <i>β</i> , <i>γ</i> (°)	90, 113.65(3), 90
Calculated density (g cm ⁻³)	5.332
Crystal colour	Transparent orange
Crystal form	Plate
Crystal size (mm ³)	0.15 × 0.11 × 0.05
Diffractometer	Bruker Smart CCD
Radiation, monochromator, temperature (K)	Mo Kα (λ = 71,073 pm), graphite, 293(2)
Ranges [2θ _{max}]; <i>h</i> , <i>k</i> , <i>l</i>	50.04°; ±14, -10 → 13, ±10
Distance detector – crystal (mm)	50
Increment, Δφ (°)	0.3
Exposure time (s)	30
Data and absorption corrections	LP and SADABS
Min./Max. transmission	0.315997/0.603229
μ (mm ⁻¹)	19.38
Measured reflections	6318
Unique reflections	977
Unique reflections, <i>F</i> ₀ > 4σ(<i>F</i> ₀)	889
<i>R</i> _{int}	0.0490
Refined parameter	64
<i>R</i> 1, <i>wR</i> 2, GooF (all Refl.)	0.0447, 0.0774, 1.193
Max. shift/esd, last ref. cycle	<0.0005
Res. electron density: max., min.	2.14, -1.23 e ⁻ (Å ³), 99, 110 pm from Ba

$$R1 = \sum ||F_0| - |F_c|| / \sum |F_0|; wR2 = [\sum w(F_0^2 - F_c^2)^2 / \sum (wF_0^2)^2]^{1/2}; w = 1/[\sigma^2(F_0^2) + (0.0082P)^2 + 24.23P] \text{ with } P = 1/(F_0^2) + 2F_c^2/3.$$

4.3. The binary alloys of the MgZn₂ type and their crystal structure

At this stage we decided to establish whether AeMg₂ compounds really were pure intermetallics or if they also contained nitrogen interstitial impurities. This possibility was considered by comparison with Ag₁₆Ca₆N [28] which is

Table 5
Ranges for the *a* and *c* lattice parameters of Ca₂N, Sr₂N and Ba₂N (literature and own results)

Compound	<i>a</i> (pm)	<i>c</i> (pm)	Reference
Ca ₂ N	361.6–363.8	1878.0–1913.8	[3,10–12]
Sr ₂ N	384.8–386.3	2061.0–2072.5	[3,13,14]
Ba ₂ N	401.3–404.6	2241.0–2269.0	[3,8,15,16]

Crystallographic data for Ae₂N are: $R\bar{3}m$ (#166), Ae on 6c with *z* ≈ 0.268 ± 2 and N on 3a.

also moderately air-stable and was believed to be the alloy Ag₈Ca₃ [29] for many years.

Previously reported crystallographic data for most of the AeMg₂ phases [5–7,21] has been derived from the refinement of Guinier powder diffractograms. The compounds AeMg₂ (Ae = Ca, Yb, Sr, Eu and Ba) are isostructural with the hexagonal Laves phase MgZn₂. In AeMg₂, Mg forms columns of corner sharing trigonal bipyramids parallel to the *c* axis and the Ae atoms are located in the channels formed by the Mg columns (Fig. 1). The Mg atoms have 6 Mg and 6 Ae nearest neighbors, while Ae have a 16-fold coordination sphere consisting of 12 Mg and a nearly perfect tetrahedron of 4 Ae closest neighbors. Emphasizing the Ae coordination, the crystal structure might also be described as hexagonal diamond analogue Ae sublattice in which the columns of corner sharing Mg₅ bipyramids are embedded. The molar volumes of the AeMg₂ compounds are slightly smaller than the sum of the atomic volumes *V*_{Ae} + 2*V*_{Mg} (Table 8). As the differences in electronegativity between the participating elements are small, the phases AeMg₂ should follow the Pauling-Simon law [31,32]. The validity of this law was demonstrated earlier for CaMg₂, SrMg₂ and BaMg₂ [33]. Fig. 2 shows a strain parameter diagram of MX₂. Laves phases formed from only electropositive metals. Their distribution over a large range of radius ratio *R*_M/*R*_N is well represented by the line [31] *y* = 0.645*x* – 0.767 (*x* = *R*_M/*R*_N, *y* = SP = [2*R*_M – *d*(MM)]/2*R*_N with *d*(MM) representing the experimentally determined mean distance between M atoms). Both EuMg₂ and YbMg₂ follow the rule

Table 4
Comparison of the crystallographic data for 'Ba₅[Ta₄N₄]' [8] and Ba₅[NbN₄]N

Stoichiometry (X-ray data)	'Ba ₅ [Ta ₄ N ₄]'	Ba ₅ [NbN ₄]N	<i>U</i> _{iso} (pm ²)
Space group (no.), Z	C2/m (12), 4	C2/m (12), 4	
Lattice constants			
<i>a</i> (pm)	1231.9(2)	1231.7(3)	
<i>b</i> (pm), β [°]	1098.5(2), 113.64(1)	1094.6(2), 113.65(3)	
<i>c</i> (pm)	855.4(1)	853.8(2)	
M (Nb or Ta), 4i	0.7536(1)/0/0.0335(2)	0.75313(11)/0/0.03353(16)	61(3)
Ba1, 4i	0.1100(2)/0/0.4059(3)	0.10874(9)/0/0.40506(13)	204(3)
Ba2, 4i	0.5509(2)/0/0.2182(3)	0.55173(7)/0/0.21960(12)	152(3)
Ba3, 4g	0/0.1782(2)/0	0/0.17841(9)/0	124(3)
Ba4, 8j	0.8219(2)/0.2723(2)/0.2763(2)	0.82238(6)/0.27315(7)/0.27828(8)	160(2)
N1, 4i	0.1865(36)/0/0.1517(56)	0.1888(12)/0/0.1496(17)	178(32)
N2, 4i	0.8751(41)/0/0.2622(64)	0.8790(13)/0/0.2618(19)	309(40)
N3, 8j	0.1479(20)/0.3629(19)/0.9991(32)	0.1486(8)/0.3615(9)/0.0011(12)	157(22)
N4, 8j, SOF: 35(5)%	–	0.0919(29)/0.2447(30)/0.3471(37)	324(85)

Table 6
Summary of the products from all reactions

Starting composition: 'AeN' or 'AeMg ₂ N ₂ ', $\sum m \approx 500$ mg	Products for $T = 600^\circ\text{C}$	Products for $T = 800^\circ\text{C}$	Products for $T = 1000^\circ\text{C}$	Products for $T = 1200^\circ\text{C}$
Mg:NaN ₃	Mg, Mg ₃ N ₂	Mg ₃ N ₂	Mg ₃ N ₂	Mg ₃ N ₂
Ca:NaN ₃	Ca, β -Ca ₃ N ₂	Ca ₃ N ₂	Ca ₃ N ₂ , Ca ₂ N	Ca ₂ N, Ca ₃ N ₂
Sr:NaN ₃	Sr ₂ N	Sr ₂ N	Sr ₂ N	Sr ₂ NbN ₃ , Sr
Ba:NaN ₃	Ba ₂ N	Ba ₂ N	Ba ₂ N	Ba ₂ NbN ₃ , Ba
Yb:NaN ₃	Yb	Yb, YbN	YbN, Yb	YbN
Eu:NaN ₃	Eu	Eu, EuN	EuN	EuN
Ca/Mg/NaN ₃	Mg, Ca, β -Ca ₃ N ₂	CaMg ₂ N ₂	CaMg ₂ N ₂	CaMg ₂ N ₂ , CaMg ₂
Sr/Mg/NaN ₃	Sr ₂ N, Mg, Mg ₃ N ₂	SrMg ₂ N ₂	SrMg ₂ N ₂	SrMg ₂ , SrMg ₂ N ₂
Ba/Mg/NaN ₃	BaMg ₂ , Ba ₂ N, Mg	Ba ₂ N, Mg ₃ N ₂ , Mg	Mg ₃ N ₂ , BaMg ₂	BaMg ₂
Yb/Mg/NaN ₃	Mg, Yb	Mg ₃ N ₂ , Yb, YbN	Mg ₃ N ₂ , YbN	YbMg ₂ , Mg ₃ N ₂ , YbN
Eu/Mg/NaN ₃	Mg, Eu	Mg ₃ N ₂ , Eu, EuN	EuN, Mg ₃ N ₂ , EuMg ₂	EuMg ₂ , Mg ₃ N ₂ , EuN
Ca ₃ N ₂ /Mg ₃ N ₂	Mg ₃ N ₂ , Ca ₃ N ₂	Ca ₃ N ₂ , Mg ₃ N ₂ , CaMg ₂ N ₂	CaMg ₂ N ₂	CaMg ₂ N ₂ , *CaMg ₂
Sr ₂ N/Mg ₃ N ₂ /NaN ₃	Mg ₃ N ₂ , Sr ₂ N	SrMg ₂ N ₂ , Sr ₂ N, Mg ₃ N ₂	SrMg ₂ N ₂ , SrMg ₂	*SrMg ₂ , SrMg ₂ N ₂
Ba ₂ N:Mg ₃ N ₂ :NaN ₃	Mg ₃ N ₂ , Ba ₂ N	Ba ₂ N, Mg ₃ N ₂	Mg ₃ N ₂ , BaMg ₂	*BaMg ₂ , Mg ₃ N ₂
YbN:Mg ₃ N ₂ :NaN ₃	Mg ₃ N ₂ , YbN	YbN, Mg ₃ N ₂	Mg ₃ N ₂ , YbN	Mg ₃ N ₂ , *YbMg ₂ , YbN
EuN:Mg ₃ N ₂ :NaN ₃	Mg ₃ N ₂ , EuN	EuN, Mg ₃ N ₂	EuN, Mg ₃ N ₂ , EuMg ₂	Mg ₃ N ₂ , *EuMg ₂ , EuN

Products were identified by their respective powder X-ray diffractograms. Metallic sodium was observed in all reactions with NaN₃. If not mentioned otherwise, the cubic α -Ca₃N₂ is referred to as ' β -Ca₃N₂'.

* Single crystals of AeMg₂ were picked from the reactions marked with an asterisk.

Table 7
Selected properties of Ae, AeMg₂, Ae–Mg–N and Ae–Nb–N compounds

Element	T_{melt} ($^\circ\text{C}$) [20]	Compound	T_{melt} ($^\circ\text{C}$) [21]	Compound	T_{react} ($^\circ\text{C}$)
Mg	649	CaMg ₂	714	Mg ₂ NbN ₃	1100 [22]
Ca	839	SrMg ₂	680	Ba ₅ NbN ₅	625
Sr	769	BaMg ₂	607	Ba ₁₆ Nb ₅ N ₁₉	950 [23]
Ba	725	YbMg ₂	718	Ba ₂ NbN ₃	1050 [24]
Yb	824	EuMg ₂	719	BaMg _{3.33} Nb _{0.67} N ₄	1025 [1]
Eu	822				
Compound	T_{react} ($^\circ\text{C}$)	Compound	T_{react} ($^\circ\text{C}$)	Compound	T_{react} ($^\circ\text{C}$)
Mg ₃ N ₂	700–900	β -Ca ₃ N ₂ [2]	$300 \leq T \leq 650$	Sr ₅ NbN ₅	900 [26]
Ca ₃ N ₂	700–900	CaMg ₂ N ₂	725 [2]		
Ca ₂ N	800–1000	CaMg ₂ N ₂	1000 [25]	Sr ₂ NbN ₃	1200 [27]
Sr ₂ N	550–700	SrMg ₂ N ₂	725 [2]		
Ba ₂ N	550–700	SrMg ₂ N ₂	950		

closely provided the radii for the rare earth elements in their lower oxidation states, 2.1 and 2.0, respectively [34], are used.

The most likely nitrogen site would be located inside the Mg bipyramids (Wyckoff position 2b), a structural motif which is also found in Mg₃BN₃ [30]. Table 8 shows that

the Mg–N bond lengths in the Mg bipyramid are plausible when compared to those found in Mg₃BN₃. The overall largest residual electron density peaks occur for the Yb, Eu and Ba compounds, but at unphysically close distances to those metal atoms. These are likely due to truncation errors of the intensity data or non-perfect absorption corrections.

Table 8
Properties of AeMg₂ compounds according to our results

Compound	$(V_{\text{mol}}/\sum V_{\text{Me}})$ (%)	$d(2b - 2a)$ (pm), $2x$	$d(2b - 6h)$, $3x$	(2b) Residual electron density (electrons/10 ⁶ pm ³)
YbMg ₂	97.1	253.0	184.2	1.07
EuMg ₂	96.7	258.1	185.2	1.20
CaMg ₂	95.0	253.6	182.6	0.21
SrMg ₂	92.1	261.4	187.6	<0.10
BaMg ₂	93.2	265.3	187.7	<0.10
Mg ₃ [BN ₂]N	–	204.6	204.0	–

Selected data for Mg₃BN₃ [30] are given for comparison.

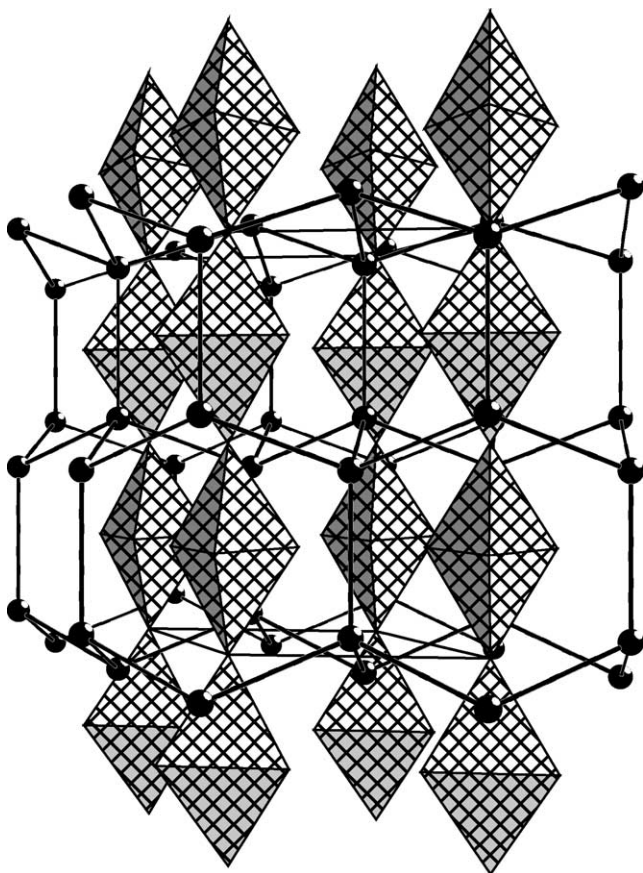


Fig. 1. View of the unit cell of $AeMg_2$ ($Ae = Ca, Yb, Sr, Eu$ and Ba) perpendicular to the c axis. $[Mg_5]$ bipyramids are drawn shaded and cross-hatched. Ae atoms (drawn as black circles) are connected with lines to emphasize the connectivity pattern resembling the hexagonal diamond structure.

For the most likely candidates $SrMg_2$ and $BaMg_2$ (which deviate most from the ideal volume and have the largest Mg_5 polyhedra) our refinement results do not exhibit significant electron densities on (2b). According to our X-ray data refinements, the maximum possible nitrogen content for all $AeMg_2$ compounds studied would be $SrMg_2N_{0.07(5)}$, that is, the nitrogen content is zero within error (Table 2).

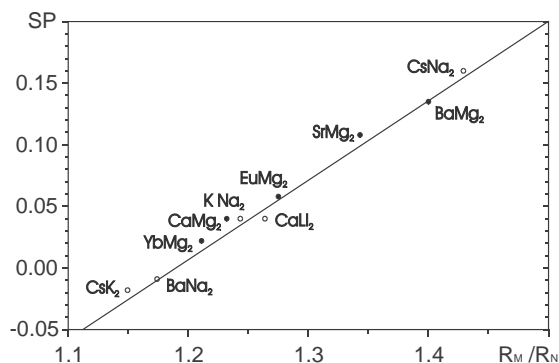


Fig. 2. Strain parameter diagram for selected Laves phases formed from only electropositive metals (filled circles refer to phases investigated in the present work). For details see text.

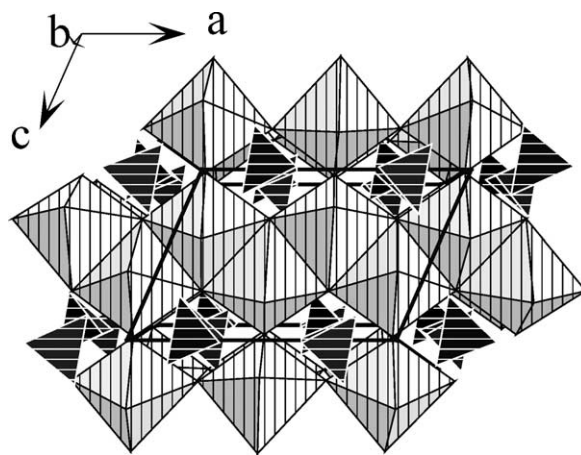


Fig. 3. View down the b axis of $Ba_5[NbN_4]N$. $[(N_4)Ba_6]$ octahedra are displayed white hatched, $[NbN_4]$ tetrahedra are shown black hatched.

4.4. Results of the crystal structure refinement of the new compound $Ba_5[NbN_4]N$

The few crystals of the new compound $Ba_5[NbN_4]N$ were all transparent orange and only of moderate crystallinity. Despite the relatively low reaction temperature employed and the sluggishness of nitrogen to react under these conditions, the $Na-Ba-N$ mixture attacked the Nb container material and incorporated the dissolved transition metal into a ternary phase.

The crystal structure of $Ba_5[NbN_4]N$ may be described as one-dimensional chains of edge sharing $[(N_4)Ba_6]$ octahedra (white hatched). The chains run parallel to the a axis (Fig. 3). The $Ba-N$ bond distances are in the expected range ($259 \text{ pm} < d < 340 \text{ pm}$, Table 9). The chains are farther interconnected via corner sharing to form sheets. These sheets are bound to each other by corner sharing the $[NbN_4]$ anions that lie between these $[(N_4)Ba_6]$ cationic layers. A projection of the unit cell of $Ba_5[NbN_4]N$ along (0 1 0) is shown in Fig. 3.

However, the refinement suggests a nitrogen deficiency on the (8j) position resulting in the formula $(Ba^{2+})_5[Nb^{5+}(N^{3-})_4](N^{3-})_{0.7(1)}$. This would imply that the electric charges are not balanced and there is an excess of approximately one electron per formula unit that is unaccounted for. Since the obtained crystals are transparent and since the refined formula $Ba_5[NbN_4]N_{0.7(1)}$ and the ideal,

Table 9
Average $Ba-N$ (all $d \leq 350$) and $Nb-N$ ($d \leq 210 \text{ pm}$) bond length of $Ba-Nb-N$ compounds

Compound	\bar{d} (Nb–N) (pm)	Range of d (Ba–N) (pm)	Reference
$Ba_5[NbN_4]N$	194.5	259.3–314.6	–
$Ba_{19}[NbN_4]_2[Nb_2N_7]$	196.0	259.1–337.8	[23]
$Ba_2[NbN_3]$	194.2	279.2–335.4	[24]
$Ba_9[NbN_4]_2N[N_3]$	197.0	261.0–336.6	[35]
$Ba_9[NbN_4]_2O[CN_2]$	196.7	261.0–336.9	[36]

ionic composition $Ba_5[NbN_4]N$ are still within the range of three standard deviations of each, it seems reasonable to assume the ideal ionic composition and to believe that the nitrogen deficiency is an artifact. There are several possible explanations for the nitrogen deficiency occurring in the refinement, e.g., the presence of heavy atoms and less than perfect absorption corrections ($R_{int} = 0.049$) and/or of the moderate crystallinity of the crystals or partial reduction of Nb. Regarding the latter point, we find that the average Nb–N bond distance in the $[NbN_4]$ tetrahedron is 194.6 pm (Table 9), which is comparable to those found in Nb(V) compounds (Table 9). Nb(IV) seems improbable since it has never been observed in a tetrahedral nitrogen environment, and one would expect the Nb–N bond length to be significantly larger in such a case. Unidentified impurities such as H, B or C must as well be considered when compounds with surprising compositions are obtained in low yield. However, neither the yield nor the quality of the crystals obtained was improved when metal powder, wire or foil were used instead of employing the container wall as the niobium source. Longer reaction times, higher reaction temperatures and/or intentionally adding reagents such as C, BaH_2 or NaH into the starting mixture resulted in the formation of $BaCN_2$, BaC_2 , $BaNH$, Ba_2NH , $Ba_{19}[NbN_4]_2[Nb_2N_7]$ or $Ba_2[NbN_3]$ as identified by powder X-ray diffraction in the respective product mixture.

Künzel reported that the compound ‘ $Ba_5[TaN_4]$ ’ formed black crystals, obtained by heating ‘ Ba_3N_2 ’ to 1400 K for 1 h in Ta ampoules [8]. A comparison with the crystallographic data reported for ‘ $Ba_5[TaN_4]$ ’ and those found by us for $Ba_5[NbN_4]N$ (Table 4) suggests that these two compounds would be isotypic if additional nitrogen on the position (8j) in the Ta compound was overlooked. However, the reported black color of ‘ $Ba_5[TaN_4]$ ’ suggests partial (or zero) occupancy of the (8j) site in the Ta compound.

5. Conclusions

A series of reactions with alkaline earth metals and nitrogen in Nb containers at different temperatures were performed. Known binary nitrides and subnitrides, the ternary nitrides $AeMg_2N_2$ ($Ae = Ca, Sr$) and ‘ β - Ca_3N_2 ’ were obtained, of which only the latter is not fully characterized. Under some conditions Nb and Ta containers are relatively inert. At higher temperatures and especially with a limited nitrogen content, the Nb walls start to participate in the reactions first by leaching out a little Nb into the reaction mixture, and then at higher temperatures by absorbing most or all of the available nitrogen leaving behind the binary alloys $AeMg_2$. Single crystal structure analyses do not indicate the presence of nitrogen on (2b) and confirm earlier results.

$Ba[Mg_{3.33}M_{0.67}]N_4$ ($M = Nb, Ta$), ‘ $Ba_5[TaN_4]$ ’ and, as reported here, $Ba_5[NbN_4]N$ were obtained first by serendipity as a by-product of reactions of alkaline earth metals with nitrogen in Nb or Ta containers. We are not yet able to prove

beyond any doubt that the composition of $Ba_5[NbN_4]N$ is exact; there is a small possibility that the N site connected only to Ba has partial occupation. However, we argue based on the transparency of the crystal that partial occupancy is unlikely.

References

- [1] O. Reckeweg, J.C. Molstad, F.J. DiSalvo, J. Alloys Compd. 315 (2001) 134–142.
- [2] O. Reckeweg, F.J. DiSalvo, Z. Anorg. Allg. Chem. 627 (2001) 371–377, and references therein.
- [3] O. Reckeweg, F.J. DiSalvo, Sol. State Sci. 5 (2002) 575–584, and references therein.
- [4] SAINT and SADABS: Bruker Analytical X-ray Instruments Software Package, Version 5.03., G. M. Sheldrick, Göttingen, 1997.
- [5] H. Witte, Naturwiss. 25 (1937) 795–800.
- [6] E. Hellmer, A. Laves, Z. Kristallogr. A 105 (1943) 134–143.
- [7] P.I. Krypyakevich, V.I. Evdakimenko, Dopov. Akad. Nauk. Ukr. SSR, 1964, pp. 766–769.
- [8] H.-T. Künzel, Doctoral Thesis, Univ. Stuttgart, Germany, 1980.
- [9] W. Klemm, G. Winkelmann, Z. Anorg. Allg. Chem. 288 (1956) 87–90.
- [10] E.T. Keve, A.C. Skapski, Inorg. Chem. 7 (1968) 1757–1761.
- [11] D.H. Gregory, A. Bowman, C.F. Baker, D.P. Weston, J. Mater. Chem. 10 (2000) 1635–1641.
- [12] C.F. Baker, M.G. Barker, A.J. Blake, Acta Crystallogr. E 57 (2001) i6–i7.
- [13] J. Gaude, P. L’Haridon, Y. Laurent, J. Lang, Bull. Soc. Fr. Min. Crystallogr. 95 (1972) 56–60.
- [14] N.E. Brese, M. O’Keeffe, J. Sol. State Chem. 87 (1990) 134–140.
- [15] O. Seeger, Doctoral Thesis, Univ. Tübingen, Germany, 1994.
- [16] V. Schultz-Coulon, Doctoral Thesis, Univ. Bayreuth, Germany, 1998.
- [17] G. Auffermann, Y. Prots, R. Kniep, Angew. Chem. Int. Ed. 40 (2001) 547–549.
- [18] Y. Prots, G. Auffermann, M. Tovar, R. Kniep, Angew. Chem. Int. Ed. 41 (2002) 2288–2290.
- [19] G.V. Vajenine, G. Auffermann, Y. Prots, W. Schnelle, R.K. Kremer, A. Simon, R. Kniep, Inorg. Chem. 40 (2001) 4866–4870.
- [20] H.W. King, in: D.R. Lide (Ed.), CRC Handbook of Chemistry and Physics, 74th ed., Chemical Rubber Publ. Co., 1993–1994, Chap. 12, pp. 10–12.
- [21] M. Hansen (Ed.), Constitutions of Binary Alloys, Genium Publ. Corporation in Arrangement with McGraw-Hill, 1985.
- [22] C. Lind, F.J. DiSalvo, unpublished results.
- [23] P. Höhn, R. Kniep, Z. Naturforsch. 56b (2002) 604–610.
- [24] O. Seeger, J. Strähle, J.P. Laval, B. Frit, Z. Anorg. Allg. Chem. 620 (1994) 2008–2013.
- [25] V. Schultz-Coulon, W. Schnick, Z. Naturforsch. 50b (1995) 619–622.
- [26] P. Höhn, R. Kniep, Z. Anorg. Allg. Chem. 628 (2002) 463–467.
- [27] Ch. Wachsmann, Doctoral Thesis, Univ. Dortmund, 1995;
- X.Z. Chen, H.A. Eick, W. Lasocha, J. Sol. State Chem. 138 (1998) 297–301.
- [28] J. Snyder, A. Simon, Angew. Chem. Int. Ed. Engl. 33 (1994) 689–690.
- [29] L.D. Calvert, C. Rand, Acta Crystallogr. 17 (1964) 1175–1176.
- [30] H. Hiraguchi, H. Hashizume, O. Fukunaga, A. Takenaka, M. Sakata, J. Appl. Cryst. 24 (1991) 286–292.
- [31] A. Simon, Angew. Chem. Int. Ed. Engl. 22 (1983) 95–113.
- [32] C.D. Churcher, V. Heine, Acta Crystallogr. A 40 (1984) 291–296.
- [33] G.J. Snyder, A. Simon, Z. Naturforsch. 49b (1994) 189–192.
- [34] W.B. Pearson, The Crystal Chemistry and Physics of Metals and Alloys, Wiley-Interscience, New York, 1972, p. 151.
- [35] S.J. Clarke, F.J. DiSalvo, Z. Kristallogr. 212 (1997) 309–310.
- [36] O. Reckeweg, F.J. DiSalvo, Z. Naturforsch. 58b (2003) 201–204.